https://doi.org/10.5194/egusphere-2026-126
Preprint. Discussion started: 27 February 2026

The SOLCHECK Project: A State-of-the-Art Investigation into the Imprints of Solar Variability Across Multiple Timescales

Tobias Spiegl[1,2], Ulrike Langematz[1], Wenjuan Huo[3], Jürgen Kröger[4], Thomas Reddmann[5], Franziska Kappenberger[1], Sebastian Wahl[3], Maryam Ramezani Ziarani[5,6], Holger Pohlmann[4] and Miriam Sinnhuber[5]

[1]Freie Universität Berlin, Institute of Meteorology, Berlin, Germany
[2]Paleoclimate dynamics, Alfred-Wegener-Institut, Bremerhaven, Germany
[3]GEOMAR, Kiel, Germany
[4]Max-Planck-Institut für Meteorologie, Hamburg, Germany
[5]Institute of Meteorology and Climate Research, Karlsruher Institut für Technologie, Karlsruhe, Germany
[6]Mathematical Institute for Machine Learning and Data Science, Katholische Universität Eichstätt-Ingolstadt, Ingolstadt, Germany

Correspondence to: Ulrike Langematz (ulrike.langematz@fu-berlin.de)

Abstract

The project *Solar Contribution to Climate Change on Decadal to Centennial Timescales* (SOLCHECK) investigated the influence of solar variability on the atmosphere from the pre-industrial era to the present and future. Variations in the Sun's output, ranging from weeks to millennia, leave distinct imprints on the climate system. Assessing these imprints is challenging due to limited observations, incomplete representation of feedbacks in climate models, and computational constraints. By exploiting a large ensemble of simulations with advanced chemistry–climate models incorporating realistic solar forcing, SOLCHECK particularly aimed at reducing prevailing uncertainties of the atmospheric solar imprints, and to assess the sensitivity of the atmospheric response to solar forcing on different time scales and in different climate states. One key result of SOLCHECK is that although the initial radiative and chemical response to the 11-year solar cycle is consistent across models in the upper tropical stratosphere, the tropospheric climate response in northern winter is highly sensitive to the dynamical state of the stratosphere, thus impeding a robust assessment of surface solar signatures and decadal climate prediction skill. Another important finding suggests that the climate system reacts differently to solar forcing under past, present, and future conditions, showing a stronger response to external solar variations in the tropical upper troposphere and the Arctic as anthropogenic warming progresses. SOLCHECK further highlighted potential impacts of extreme solar storms in a future climate, as such events, although occurring

https://doi.org/10.5194/egusphere-2026-126
Preprint. Discussion started: 27 February 2026

extremely seldom, may have substantial effects on surface UV with potential consequences for ecosystems and human health.

1 Introduction

While the influence of human activity on climate since industrialization is undeniable, natural climate drivers may not be ignored, as they continue to shape our climate system over various timescales. Distinguishing between anthropogenic and natural factors not only deepens our understanding of Earth's complex system but also enhances both short- and long-term climate predictions. Among the natural forces, the Sun plays an important role, influencing Earth's energy balance and atmospheric composition with fluctuations ranging from days to centuries (e.g., Coddington et al., 2019).

An extreme form of solar variability are large solar storms, including coronal mass ejections and solar flares. They eject plasma into interplanetary space and trigger enhanced precipitation of high-energy protons at high geomagnetic latitudes—the so-called solar proton events (SPEs). SPEs strongly disturb middle-atmospheric chemistry, initiating odd nitrogen (NO_y) production in the mesosphere and lower thermosphere and causing ozone loss in the high-latitude upper stratosphere via radiative–chemical feedbacks (Sinnhuber et al., 2012, 2018, 2019). These effects can influence atmospheric dynamics and wintertime tropospheric weather (Seppälä et al., 2009; Maliniemi et al., 2014, 2019). During the satellite era, major SPEs such as the 2003 Halloween storm occurred each solar maximum, altering the global stratospheric NOy budget with implications for the ozone layer above ~30 km (Randall et al., 2007; Funke et al., 2014; Sinnhuber et al., 2018). Paleonuclide records show that much stronger SPEs occurred repeatedly over the last 10,000 years (Usoskin 2023; Usoskin et al., 2023). In SOLCHECK, such events were investigated with EMAC and KASIMA to assess ozone depletion, ultra violet (UV) related health impacts, and chemistry–radiation–dynamics coupling.

A well-known form of solar variability is the 11-year solar cycle, with total solar irradiance (TSI) variations of ~1 W/m² (~0.7 ‰) (Grey et al., 2010), while spectral solar irradiance (SSI)—especially in the UV—shows stronger fluctuations. UV variability affects the thermal structure of the tropical upper stratosphere, where interactions between shortwave radiation and ozone alter meridional temperature gradients and trigger circulation anomalies. These anomalies can propagate downward into the troposphere via interactions with upward planetary waves during boreal winter (Kodera, 2002; Kodera and Kuroda, 2002), a pathway commonly referred to as the "top-down" mechanism in subsequent studies. Some studies suggest that solar signals synchronize the decadal

https://doi.org/10.5194/egusphere-2026-126
Preprint. Discussion started: 27 February 2026

component of the North Atlantic Oscillation (NAO) (Thiéblemont et al., 2015) and improve North Atlantic winter prediction skill (Drews et al., 2022), whereas others challenge this (Chiodo et al., 2019; Spiegl et al., 2023). To address these discrepancies, SOLCHECK carried out a large historical-like CMIP6-type ensemble using the chemistry-climate models (CCMs) EMAC and FOCI and the MiKlip decadal prediction system, enabling assessment of the combined and individual impacts of the 11-year cycle and longer-term solar trends.

On centennial scales, Grand Solar Maxima and Minima (GSM) involve suppressed solar cycles or reduced solar output, with at least five such events over the past millennium (Usoskin et al., 2009). The Maunder Minimum (1645–1715) (Eddy, 1976) coincided with Europe's Little Ice Age (LIA), featuring severe winters (Zorita et al., 2004) and hot, humid summers (Rimbu et al., 2024). Evidence suggests the current Grand Solar Maximum is ending (de Jager et al., 2016), potentially leading to GSM-like conditions in coming decades (Rahmanifard et al., 2022). While previous studies assessed whether a modern GSM could slow anthropogenic climate change (e.g., Spiegl & Langematz, 2020; Sedlacek et al., 2023), the SOLCHECK EMAC simulations examine how anthropogenic changes from the pre-industrial era to the future may modulate such centennial solar signals via shifts in the atmospheric background state.

2 Extreme solar particle events: Impact on Earth's atmosphere in modern times

One of the SOLCHECK goals was to investigate the atmospheric and societal impacts of a worst-case SPE in modern times. For this purpose, a scenario based on isotopic records of the 774/775 CE SPE was chosen (Miyake et al., 2012; Mekhaldi et al., 2015), the strongest ground-level event of the past 10,000 years with an estimated proton flux 50–100 times larger than the largest space-era event in 1956. Because SPEs can trigger geomagnetic storms, ionization rates for an extreme geomagnetic storm occurring two days after the eruption were included. A second event of interest was the October 2003 "Halloween" storm, one of the strongest modern SPEs. SPEs and geomagnetic storms affect the middle atmosphere most during polar winter, when NO_y formed in the mesosphere–lower thermosphere is transported into the upper stratosphere (e.g., Sinnhuber et al., 2012, 2018).

Two models were used: a) the mechanistic KArlsruhe SImulation Model of the middle Atmosphere (KASIMA; Kouker et al., 1999), driven by observed dynamical fields and suitable for sensitivity studies under specific meteorological conditions. This allowed determination of the direct chemical and UV impact of a 774/775 CE-like SPE under conditions maximizing vertical coupling between the mesosphere-lower thermosphere (MLT) region and the stratosphere, such as during strong sudden stratospheric warmings (SSWs). The Northern

https://doi.org/10.5194/egusphere-2026-126
Preprint. Discussion started: 27 February 2026

Hemisphere (NH) winter 2008/2009 SSW provided the dynamical input for the KASIMA study (Reddmann et al., 2023). b) The ECHAM/MESSy configuration B (EMAC-B) chemistry-climate model (see Supplement) was used to identify dynamical feedbacks of an extreme 774/775 CE-like and a "Halloween" SPE under present-day conditions. To obtain statistically robust dynamical responses, 19 ensemble members were performed for each scenario.

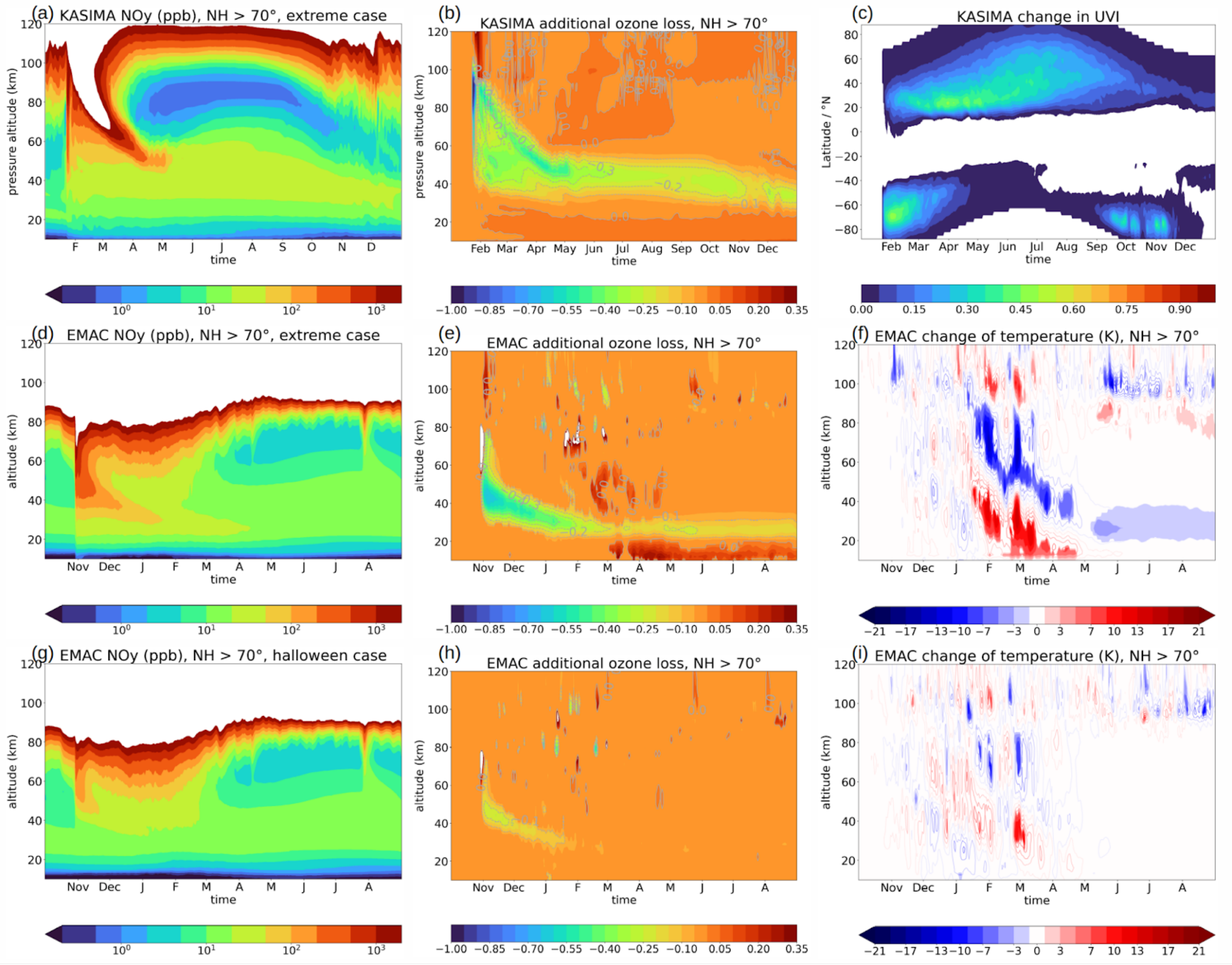

Figure 1: Model results for extreme solar proton events. Uppermost panel: KASIMA with specified dynamics. Middle and lower panels: ensemble mean of 19 members, EMAC-B. Left panels: NO_y mixing ratio in the model experiments with SPE, from top to bottom: "extreme" event during a SSW in January 2009; extreme event in late October 2003; "Halloween" storm event of late October 2003. Middle panels: ozone change relative to a "quiet"

scenario without SPE. Right panels: Top: Change in surface UV due to the extreme event during the January 2009 SSW; middle and bottom: change in temperature compared to the quiet scenario for extreme SPE and Halloween SPE of October 2003. Filled contours in panels (f) and (i) are 3-sigma significant considering the standard error of the reference ensembles. KASIMA results are adapted from Reddman et al., 2023.

Figure 1 summarizes the major results. Independent of timing, the extreme SPE increases NO_y by up to three orders of magnitude from the mid-stratosphere to the lower thermosphere, with enhancements even below 20 km (Fig. 1a, 1d). If such an event coincides with a strong SSW, downward transport into the stratosphere is greatly amplified. By contrast, the Halloween SPE produces only a 1–2 order-of-magnitude NO_y increase, confined above 40 km (Fig. 1g). Most NO_y originates from the SPE, while geomagnetic-storm effects remain limited to high altitudes. In all scenarios, SPE-produced NO_y is long-lived, descends during polar winter, and drives substantial ozone loss. For the extreme events, ozone loss exceeds 40% at 40 km and persists into the following summer (Fig. 1b, e), whereas the Halloween storm yields up to 25% loss restricted to winter (Fig. 1h). During an extreme SPE with SSW, ozone loss reaches 50% initially, with recovery to ~80% within one year. The long-lasting ozone reduction increases UV erythema dose by <5% at mid and low latitudes (Fig. 1c) and induces mid-stratospheric cooling at high latitudes. The October extreme event also produces significant high-latitude temperature anomalies (Fig. 1f), suggesting an earlier polar-vortex breakdown, with the Halloween storm showing a similar but weaker pattern (Fig. 1i). These findings demonstrate that SPEs can exert a reproducible wintertime stratospheric impact, although events far exceeding space-era intensity are required to overcome large internal variability. The confinement of responses to the stratosphere highlights the atmosphere's resilience to extreme solar disturbances, with implications for exoplanet habitability under strong particle forcing (Siskind et al., 2024).

3 The 11-year solar cycle: Impact on stratospheric and tropospheric dynamics

3.1 11-year solar signals in different atmospheric domains and their uncertainties

To quantify the contribution of the 11-year solar cycle to decadal climate variability is essential for near-term climate prediction and attribution. . However, the transfer of the solar signal from the upper stratosphere to the surface and its impact on the troposphere and oceans remain under debate. The “top-down mechanism” proposed by Kodera and Kuroda (2002) provides a theoretical framework, yet models differ in their representations. To investigate this, the SOLCHECK models FOCI and EMAC (configuration A, with interactive ozone) and MPI-ESM-HR (with prescribed ozone) were applied. Two CMIP6 ensemble sets with identical anthropogenic greenhouse gas (GHG) and ozone depleting substances (ODS) forcing—but either including the 11-year solar cycle or prescribing constant solar forcing (“FULL” and “FIX”)—were performed for 1850–2014.

The 11-year solar imprints in shortwave heating rates (SWHR), temperature, and ozone (O_3) were analysed as the “initial signal” for a wintertime dynamical response via modulation of meridional temperature gradients. Figure 2a shows composite differences between solar maxima and minima in annual-mean tropical SWHR profiles. Using FIX simulations as a reference, a clear solar signal appears in all models when solar forcing is included. Enhanced solar heating during solar maximum induces stratospheric and lower mesosphere warming of about 0.30–0.45 K around the stratopause (Fig. 2b). The strongest O_3 response (Fig. 2c) occurs in the middle stratosphere due to enhanced ozone production.

The initial radiative responses in SWHR and O_3 are robust and consistent. Internal spread is small, and all models agree on the vertical structure and height of the SWHR and O_3 maxima. Remaining amplitude differences arise from model-specific shortwave radiation schemes. Ozone responses compare well, with larger spread in FOCI linked to dynamical ozone transport. In MPI-ESM-HR, O_3 is prescribed, so no interactive chemistry contributes to the temperature signal.

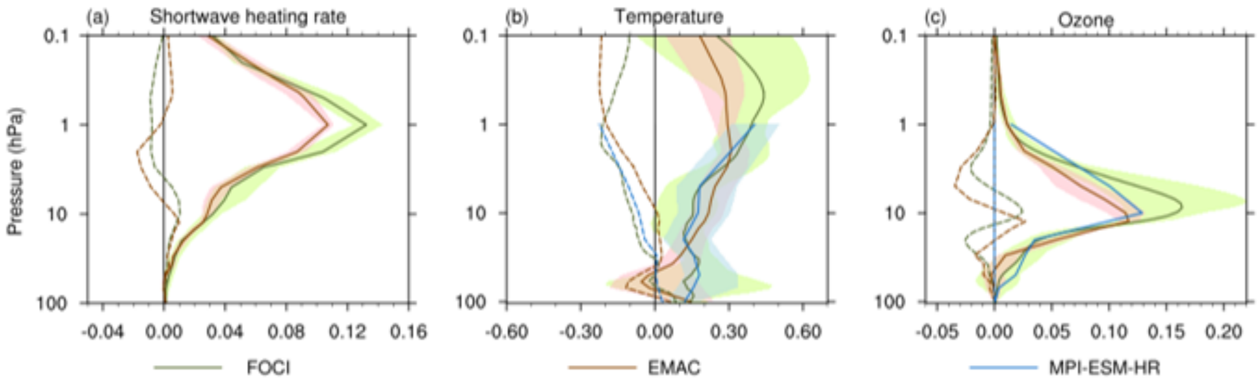

Figure 2: Composite differences between solar maxima and minima of the annual and tropical (over 25°S–25°N) mean (a) short wave heating rates (in K/day) in the FULL (solid lines) and the FIX (dashed lines) ensemble mean with FOCI (green) and EMAC (red). Light green and light red shading indicate the ensemble spread in FOCI and EMAC respectively. (b) same as (a), but for air temperature (in K) from FOCI (green), EMAC (red), and

MPI-ESM-HR (blue). Light blue shading represents the ensemble spread in MPI-ESM-HR. (c) same as (b), but for ozone (O_3) volume mixing ratio (in ppmv).

In contrast, the temperature response (Fig. 2b) shows much larger ensemble spread in all models, indicating greater uncertainty in solar-induced anomalies and strong interference from internal variability. Differences in the vertical profile of the temperature response further suggest that internal model dynamics play a key role. Thus, while the radiative upper-stratospheric solar signal is consistently captured, its downward propagation—and the resulting tropospheric influence—remains model dependent.

The above findings are further illustrated by timeseries of tropical stratopause temperature and zonal-mean zonal wind averaged over 55°N and 65°N (Fig. 3). A consistent decadal variation and phase-locking to the 11-year solar cycle appear in all SOLCHECK simulations with solar forcing, and most clearly in the multi-model ensemble mean (MME). However, uncertainty in the dynamical response is much larger than in the thermal response, and no consistent solar imprint emerges in December zonal-mean zonal wind. Doubling the solar cycle amplitude in a FOCI sensitivity experiment enhances tropical stratopause temperature variability, but detectability of solar signals in zonal-mean wind or surface fields does not scale linearly, indicating that ensemble-mean linear responses represent only a small part of the dynamical signal.

In summary, the "top-down mechanism" could not be consistently reproduced. While the radiative signal at the tropical stratopause is robust, the polar vortex response varies strongly between models and individual ensemble members, explaining the non-robust "top-down" and surface responses.

https://doi.org/10.5194/egusphere-2026-126
Preprint. Discussion started: 27 February 2026

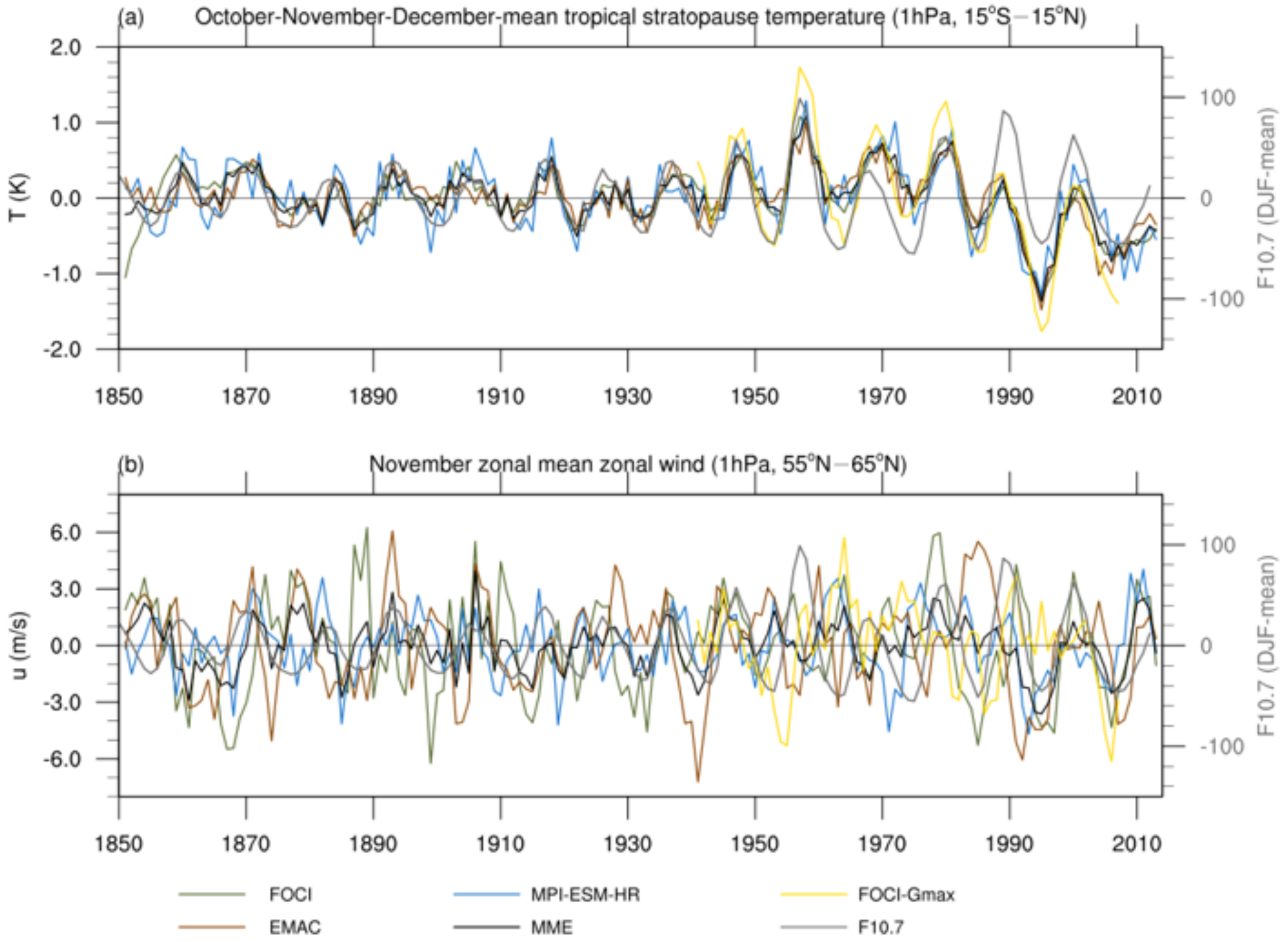

Figure 3: (a) Time series of the October-November-December mean tropical stratopause temperature (1hPa, 15°S–15°N) for the ensemble means of the historical simulations with FOCI (green), EMAC (red), and MPI-ESM-HR (blue), respectively. The black line indicates the multi-model ensemble mean and the grey line represents the F10.7 index. The golden line is the ensemble mean in the experiment with doubled solar amplitude with FOCI (FOCI-Gmax, more details can be found in section A2.2). (b) Same as (a), but for November zonal mean zonal wind at 1hPa averaged over 55°N–65°N.

3.2 The 11-year solar cycle: Impact on decadal prediction skill

The impact of solar variability on climate predictions is assessed using the German decadal climate prediction system MiKlip (Marotzke et al., 2016). Ensemble simulations with the MiKlip system, with and without solar variability, estimate solar contributions to decadal climate prediction skill. MiKlip contributes to the Decadal Climate Prediction Project (DCPP; Boer et al., 2016) of CMIP6 (Eyring et al., 2016). The 10-year retrospective forecasts, consisting of 10 ensemble members with the MPI-ESM-HR model (Müller et al., 2018), were initialized from observations every November 1st over the period 1960–2013 (Pohlmann et al., 2019). The SOLCHECK ensemble differs from DCPP predictions in its solar forcing, which only includes the annual cycle of 1850 with no long-term variability. The prediction quality with full solar forcing (including the 11-year solar cycle) is evaluated by the correlation skill score (CSS) of the multi-annual mean surface air temperature forecast for two to five years (Figure 4). Experiments without solar variability serve as a reference for skill score calculation, using observed surface temperatures from the GISTempv4 dataset (Lenssen et al., 2019). A positive skill score indicates improved forecast quality attributed to solar radiation. Significant improvements are observed in polar regions and selected land areas like the Antarctic Peninsula and the Pacific Northwest region, parts of eastern Russia and eastern China, Mongolia and Turkey, North African regions around Algeria, Tunisia and Egypt, and parts of France, Venezuela, Suriname and Brazil. A mix of neutral conditions and positive skill scores in large areas of the tropical and subtropical Pacific Ocean suggests a potential solar influence on predicting the El Niño Southern Oscillation (ENSO) phenomenon, although improvements in the eastern equatorial Pacific, the core of ENSO, are not significant. In summary, as opposed to significant improvements all over the globe, there is little significant worsening of forecast quality detectable when including the solar forcing as can be seen, e.g., in and around the Great Australian Bight.

https://doi.org/10.5194/egusphere-2026-126
Preprint. Discussion started: 27 February 2026

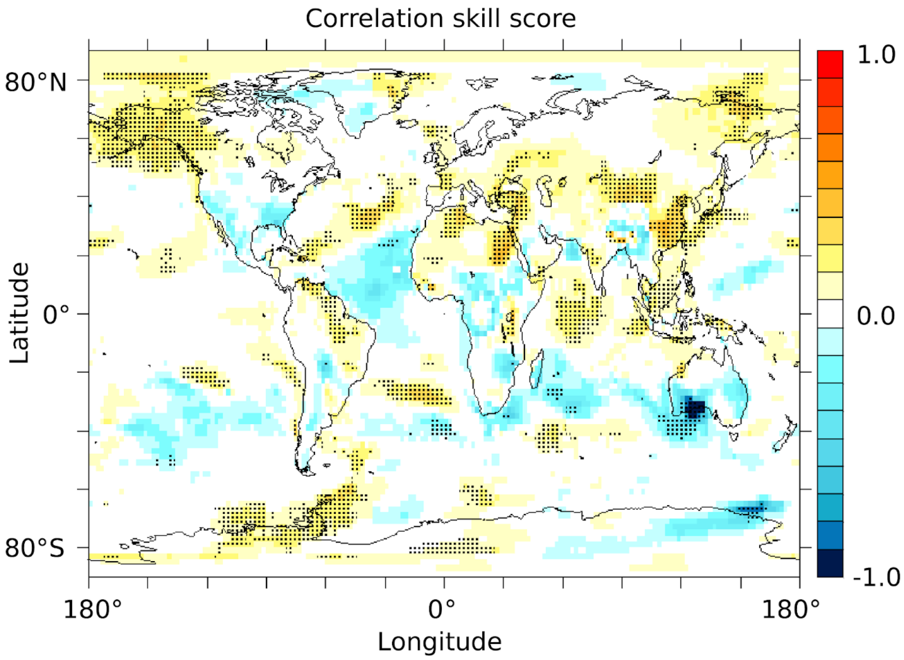

Figure 4: Correlation skill score (CSS) of the multi-annual mean surface air temperature for the forecast horizon 2 to 5 years of the ensemble forecasts, each initialised on November 1st from 1960 to 2013. Comparison of the DCPP decadal forecasts to the forecasts with suppressed variability in solar forcing. Correlations were determined using observations from GISTempv4 (Lenssen et al., 2019). Points indicate 95% significance, determined via bootstrap sampling.

4 Grand Solar Minimum: Impact on the climate system under past, present and future atmospheric boundary conditions

While already early GCM studies (Rind et., 1999; Langematz et al., 2005) investigated whether a reduction in solar energy could explain the cooling during the later stages of the Little Ice Age (Luterbacher et al., 2005), the perspective in SOLCHECK has been shifted. Here, the aim was to determine whether an identical solar downturn would unfold differently under altered atmospheric conditions across different climate periods.

To examine GSM fingerprints, timeslice simulations were performed with the SOLCHECK model EMAC (configuration A) including interactive ocean coupling, using atmospheric boundary conditions representative of

https://doi.org/10.5194/egusphere-2026-126
Preprint. Discussion started: 27 February 2026

1850, 2020, and 2100. For each period, a reference simulation with constant solar irradiance (CMIP6 piControl; Matthes et al., 2017) and a simulation with a strong GSM-like reduction in TSI and corresponding SSI changes (Egorova et al., 2018) were conducted.

Figure 5 summarises temperature responses in the atmosphere and ocean for increasing GHG concentrations. Differences between the 2100 and 1850 reference states (top row) show characteristic anthropogenic climate features: strong tropospheric warming with a tropical upper-tropospheric hotspot and cooling above (Fig. 5a), pronounced NH surface warming due to Arctic Amplification (Fig. 5b), and substantial ocean warming in the upper 2,500 m (Fig. 5c). The 2nd–4th rows of Figure 5 display the GSM-induced cooling under 1850, 2020, and 2100 conditions. While the solar forcing reduction is identical, the climate response strengthens with progressing anthropogenic warming. GSM cooling is significantly stronger under 2100 conditions (Fig. 5f, i, l), particularly in the tropical upper troposphere (Fig. 5d, g, j) and NH polar regions at the surface (Fig. 5e, h, k). Ocean cooling also intensifies and penetrates into deeper layers in 2100. These enhanced GSM effects arise from changes in Earth’s thermal state and associated feedbacks. In the Arctic, reduced sea ice under warming exposes open water to diminished solar input during a GSM which cools the atmosphere and surface waters, promoting sea ice regrowth. Increased winter sea ice insulates the cold atmosphere, reinforcing the cooling, which persists into spring through enhanced albedo. In the tropics, a reduced lapse rate under anthropogenic warming alters cloud structure and composition, which allows for more reflection of the already reduced solar radiation, further amplifying GSM cooling.

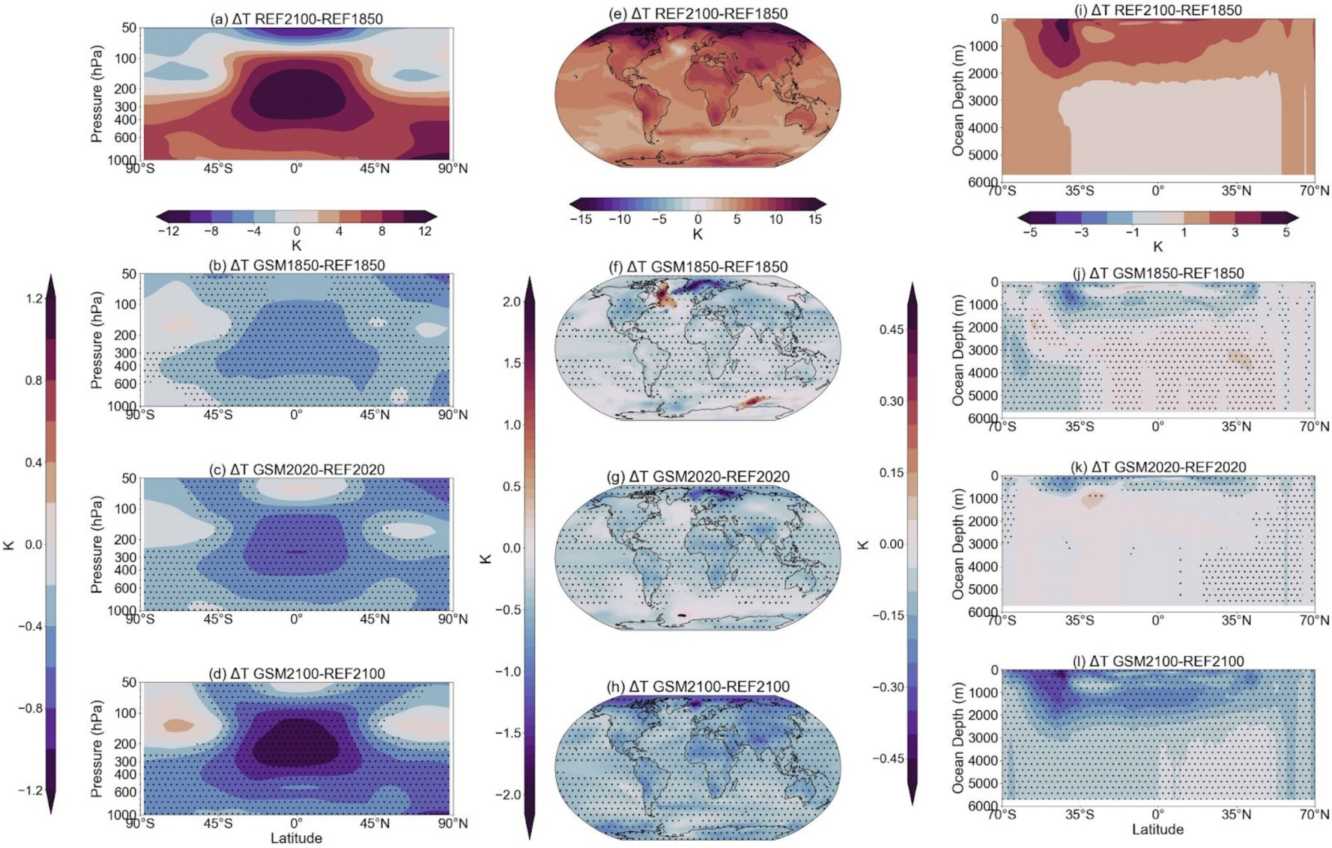

Figure 5: Temperature changes across different domains of the climate system due to climate change and a GSM. 1st row: Climate change from 1850 to 2100 assuming pre-industrial solar forcing. (a) Long-term annual and zonal mean temperature in the troposphere and lower stratosphere, (b) 2m temperature, and (c) zonal-mean ocean temperature. All anomalies are significant at the 99% confidence level according to a Student's t-test. 2nd–4th row: Fingerprint of the GSM. (d, e, f): temperature anomaly due to GSM for the same variables as in (a, b, c) under GHG concentrations of 1850. (g ,h, i) same as (d, e, f) but under anthropogenic forcing of 2020. (j, k, l): same as (d, e, f) but under anthropogenic forcing of 2100. Stippled areas indicate regions where the GSM signals are statistically significant at the 99% confidence level based on a Student's t-test.

5 Conclusions

The main goal of the SOLCHECK project was to investigate the influence of solar variability on the climate system from decadal to centennial timescales. Using a unique, large ensemble of coordinated simulations with advanced CCMs and an ESM that incorporated realistic solar variability, SOLCHECK addressed several open questions regarding the solar impact on climate.

Our results show that extreme solar proton events, such as the 774/775 CE event, can cause dramatic increases in NO_y and substantial ozone depletion, particularly during polar winter. Ozone loss exceeded 40% around 40 km, with effects on UV radiation and mid-stratospheric temperatures that persisted into the following summer. However, such strong impacts occurred only in scenarios with solar storms far more intense than those observed during the satellite era, highlighting the need to consider extreme solar events in climate model integrations. Future studies should examine long-term consequences for ecosystems and human health.

We also found that initial solar signals of the 11-year solar cycle—changes in shortwave heating rates and ozone anomalies in the upper tropical stratosphere—are consistent across models. In contrast, the polar vortex response varies strongly, suggesting that its background state modulates sensitivity to solar-cycle forcing. Further work is needed to clarify how this background state influences the downward propagation of solar signals and how this affects decadal climate prediction skill.

A third key result concerns the response to a Grand Solar Minimum (GSM). The climate system reacts differently under past, present, and future conditions. In a future (2100) scenario, GSM-induced cooling is considerably stronger, particularly in the tropical upper troposphere and the Arctic. This increased sensitivity suggests that, as anthropogenic warming progresses, the climate system may respond more strongly to external solar variations or internal perturbations such as volcanic eruptions. These insights are also relevant for interpreting paleoclimate periods influenced by elevated greenhouse gas levels.

Data availability

The main SOLCHECK project data are freely available via the links below.

https://www.wdc-climate.de/ui/q?query=SOLCHECK&page=0&rows=15

https://doi.org/10.35097/1104

https://doi.org/10.5194/egusphere-2026-126
Preprint. Discussion started: 27 February 2026

Model results of the extreme solar scenario with the KASIMA model are available at https://radar.kit.edu/radar/en/dataset/izqpNGXyOJDYMKfc. Model results of the extreme solar scenario and the Halloween storm with the EMAC configuration B model will be made available on radar.kit.edu before publication.

Appendix: Data and methods

Appendix A: Model descriptions, experimental setup and analysis

In the following, we first describe the chemistry–climate and Earth system models that contributed to SOLCHECK, whose outputs form the basis of our analysis. We then discuss the experiments presented in the main text and explain the analytical methods used.

A1 Model descriptions

FOCI:

The Flexible Ocean Climate Infrastructure (FOCI; Matthes et al., 2020) integrates several components, including the high-top European Centre Hamburg general circulation model, sixth generation (ECHAM6.3) (Stevens et al., 2013), which is coupled to the Nucleus for European Modelling of the Ocean (NEMO3.6) (Madec, 2016), the JSBACH land module (Reick et al., 2013), and the Louvain-la-Neuve Sea Ice Model (LIM2) (Fichefet and Maqueda, 1997). For the atmospheric model, FOCI employs the T63L95 configuration of ECHAM6.3, which features 95 hybrid sigma–pressure levels extending up to 0.01 hPa and a horizontal resolution of approximately 1.8° × 1.8°. The ocean model uses a nominal global resolution of 1/2° with 46 vertical levels in the ORCA05 configuration (Biastoch et al., 2008). To simulate atmospheric chemical processes, FOCI incorporates the Model for Ozone and Related Chemical Tracers (MOZART3; Kinnison et al., 2007) within ECHAM6 (ECHAM6-HAMMOZ; Schultz et al., 2018), using a simplified chemistry scheme designed for stratospheric applications. This scheme includes 48 chemical tracers and accounts for 185 reactions, including 50 photolysis reactions. Radiative transfer is represented using the Rapid Radiative Transfer Model (RRTMG) (Iacono et al., 2008). Further details on the simplified chemistry scheme are provided in Schmidt et al. (2006). The quasi-biennial oscillation (QBO) is internally generated by the model.

EMAC in configuration A (hereafter referred to as EMAC-A):

The ECHAM/MESSy chemistry-climate model (EMAC) (ECHAM5 Version 5.3.02, MESSy Version 2.52) is designed to simulate processes in the troposphere and middle atmosphere, including their interactions with oceans, land surfaces, and human-induced factors (Jöckel et al., 2010). EMAC is built on the Modular Earth Submodel System (MESSy2), integrating various software components from different research institutions, with the ECHAM5 model (Roeckner et al., 2006) serving as the core for atmospheric simulations. For the SOLCHECK project, EMAC was set up in a T42L47MA configuration, which corresponds to a 2.8° x 2.8° grid and 47 vertical layers, with the top of the model at 0.01 hPa. Key submodels for this project include MECCA (Sander et al., 2011) for atmospheric chemistry, JVAL (Sander et al., 2014) for photolysis rates, and a streamlined version of the tropospheric chemistry to enhance model efficiency. The chemical mechanism follows the detailed CCMI-base-02 setup (Jöckel et al., 2016) for stratospheric and mesospheric processes, but a simplified tropospheric chemistry scheme was adopted to improve model performance. The applied chemical mechanism considers 98 chemical tracers and a total of 156 reactions, including 50 photolysis reactions. Additional submodels used in the simulations include QBO (Giorgetta and Bengtsson, 1999), UBCNOx (Funke et al., 2016) for auroral effects, and MPIOM (Jungclaus et al., 2006) for ocean dynamics at GR15L40 resolution (1.5° grid, 40 levels). To enhance the model's UV–VIS spectral resolution, the FUBRAD submodel (Kunze et al., 2014) was employed for the stratosphere and mesosphere below 70 hPa, using 81 spectral bands that cover key features, including the Lyman-α line (121.5 nm), Schumann–Runge bands (125.5–205 nm), Herzberg continuum (206.2–243.9 nm), Hartley bands (243.9–277.8 nm), Huggins bands (277.8–362.5 nm), and Chappuis bands (407.5–690 nm).

EMAC in configuration B (hereafter referred to as EMAC-B):

To investigate the impact of an extreme solar event on atmospheric composition and dynamics, EMAC was used in an alternative configuration. In this setup, the model resolution T42L74 was applied, with the model top placed in the lower thermosphere at 3×10^{-7} hPa (~200 km). This configuration is described in detail in Sinnhuber et al. (2021). An updated version not yet used here is described in Sinnhuber et al. 2025. . In addition to the standard configuration, the submodules EDITH (Sinnhuber et al., 2021; Sinnhuber et al., 2025) and SPE (Baumgaertner et al., 2010; Sinnhuber et al., 2021, 2025) were activated. These submodules provide parameterizations for non-LTE radiative cooling, Joule heating, molecular diffusion, as well as EUV and particle-impact ionization, together with a simplified ion chemistry scheme (see Sinnhuber et al., 2021, 2025). Ionisation rates for electrons, protons and alpha particles with a 2 hour resolution are taken from the AIMOS model (Wissing and Kallenrode, 2009) with the exception of three days in the “extreme” scenario, where ionization rates from Reddman et al., 2023 are used.

The radiative transfer scheme FUBRAD was employed with a slightly reduced spectral resolution using 55 bands. The chemical setup is based on a subset of the CCMI-Base02 mechanism (Jöckel et al., 2016) in its stratospheric configuration, comprising 94 species and 2659 reactions, including 46 photolysis, and 20 heterogeneous reactions. In addition, it includes positive ions (N^+, N_2^+, O^+, O_2^+, NO^+), electrons, negative charge, and the short-lived excited state $N(^2D)$ as described, e.g., in Sinnhuber et al., 2021.

KASIMA:

The KArlsruhe SImulation Model of the middle Atmosphere (KASIMA; Kouker et al., 1999) is a mechanistic model solving the meteorological basic equations in spectral form in the altitude range between 300 hPa and $3.6 \times 10{-}5$ hPa., with the pressure height $z = H \log(p/p0)$ ($H = 7$ km and $p0 = 1013.25$ hPa) as a vertical coordinate. It uses radiative forcing terms for UV–Vis and IR as well as a gravity wave drag scheme. In order to yield a realistic meteorology, the model is relaxed (nudged) to ERA-Interim meteorological analyses (Dee et al., 2011) between the lower boundary of the model and 1 hPa. A full stratospheric chemistry including heterogeneous processes is adapted to include source terms related to particle ionization. The model participated in the three model-data inter-comparisons, initiated by the High Energy Particle Precipitation in the Atmosphere (HEPPA) initiative within the former Stratosphere-troposphere Processes And their Role in Climate (SPARC) World Climate Research Programme (Funke et al., 2011a, 2017; Sinnhuber et al., 2021). The model has proven to realistically simulate the chemistry and dynamics of NO_y intrusions into the middle atmosphere for studying their direct impact on the chemical state of the middle atmosphere. The model was used in the version described in Sinnhuber et al. (2021) in more detail.

MPI-ESM:

The coupled Max Planck Institute Earth System Model is used in the MPI-ESM1-2-HR configuration (Müller et al., 2018). Its individual components include the atmospheric general circulation model ECHAM6.3 (Stevens et

https://doi.org/10.5194/egusphere-2026-126
Preprint. Discussion started: 27 February 2026

al., 2013) on a spectral grid with triangular truncation T127, coupled to the ocean model MPIOM1.6.2 (Jungclaus et al., 2013) on a 0.4° tripolar grid with 40 vertical levels. The ocean biogeochemistry is represented by the Hamburg Model of the Ocean Carbon Cycle (HAMOCC; Ilyina et al., 2013), and land processes are described by the JSBACH model (Reick et al., 2013). Ozone concentrations from CMIP6 are prescribed as boundary conditions for the model integrations (Hegglin et al., 2016). Additional boundary forcings include annual and global mean greenhouse gas concentrations (Meinshausen et al., 2017), anthropogenic aerosols (Fiedler et al., 2017; Stevens et al., 2017), volcanic aerosols (Thomason et al., 2018), and spectral solar irradiance (Matthes et al., 2017). Radiative transfer in ECHAM6.3 is calculated using the Monte Carlo Independent Column Approximation (Pincus & Stevens, 2013). The atmospheric vertical resolution comprises 95 levels, with a well-resolved stratosphere extending to 0.01 hPa, allowing for a freely evolving quasi-biennial oscillation (Giorgetta et al., 2006; Pohlmann et al., 2019).

A2 Experimental setup and analysis

A2.1 Extreme solar particle event simulations and analysis

To model the impact of an extreme solar particle event, ionization rates were prescribed for three days, combining an extreme solar event consistent with the AD 774/775 event on the first day with an extreme geomagnetic storm on the third day, as described in Reddmann et al. (2023). Three model experiments were conducted with EMAC-B and KASIMA over different time periods. For EMAC-B, simulations were performed for the period of the Halloween solar storm from late October 2003 through the subsequent polar winter. KASIMA simulations were carried out for the polar winter 2008/2009, which included a very strong SSW in January followed by pronounced downwelling in the newly formed polar vortex, aiming to highlight the interplay between two extreme events: the extreme solar particle event and the extreme dynamical situation following the SSW. Three model experiments were performed with EMAC-B: a reference simulation without a solar particle event, a simulation including the observed Halloween 2003 solar storm, and a simulation of an AD 774/775–like extreme solar particle event. Except for the extreme solar particle event itself, ionization rates from the AISstorm model (see, e.g., Sinnhuber et al., 2021, and references therein) were prescribed. Nineteen ensemble members were carried out for each of the three experiments. KASIMA performed three model experiments using ionization rates

https://doi.org/10.5194/egusphere-2026-126
Preprint. Discussion started: 27 February 2026

from the AIMOS model (Wissing and Kallenrode, 2009), the precursor to Aiststorm: a reference run without an extreme event, a run including the extreme event on 21–23 January 2009 at the onset of the SSW, and a sensitivity run in which the extreme solar event occurred on 21 January but without the extreme geomagnetic storm on the third day.

A2.2 11-year solar cycle simulations and analysis

Two sets of CMIP6 historical-like ensemble simulations were conducted using three climate models (FOCI, EMAC-A, and MPI-ESM-HR), all driven by the same external forcings as recommended for CMIP6 (Eyring et al., 2016), with the exception of solar forcing. The first ensemble, referred to as FULL in this study, incorporates full solar variability based on the CMIP6 solar forcing dataset (Matthes et al., 2017). The second ensemble, termed FIX, serves as a reference in which the solar forcing is held constant at the mean value over the years 1850–1873. All simulations, across all three models, cover the historical period from 1850 to 2014. Each ensemble member is initialized from different model years of a multi-centennial pre-industrial control simulation. In total, 9 members of the FULL ensemble were run with FOCI, 6 with EMAC-A, and 10 with MPI-ESM-HR, yielding 25 members and 4125 model years analyzed in this study. The FIX ensemble contains the same number of members as the FULL ensemble for FOCI and EMAC-A, and 8 members for MPI-ESM-HR.

In addition, a set of sensitivity experiments (9 members in total) was performed with FOCI, driven by a modified solar forcing with doubled solar cycle amplitudes during the period 1940–2008, referred as FOCI-Gmax in this studyThe solar forcings were constructed by scaling the full CMIP6 solar forcing (used as the reference), keeping solar minima unchanged while doubling the amplitude of each solar cycle. All other external forcings match those used in the historical-like experiments.

To extract the imprint of the 11-year solar cycle, we calculated the composite mean difference (CMD) between solar-cycle maxima and minima (Camp and Tung, 2007) for selected meteorological variables. Solar maxima (minima) were identified following Drews et al. (2022): as the peaks (valleys) of the 3-year smoothed December–January–February (DJF) mean F10.7 index together with the two years surrounding each peak (valley). We then computed the difference between the average values in all solar-maximum and solar-minimum years.

https://doi.org/10.5194/egusphere-2026-126
Preprint. Discussion started: 27 February 2026

Furthermore, a correlation skill score (CSS) was calculated that can be used to directly reveal gains and losses in prediction skill due to the solar cycle. The skill score calculation requires a reference forecast, which for our purpose is the ensemble hindcasts (or retrospective forecasts) with constant solar forcing. The CSS for the hindcasts with full solar forcing is now calculated from anomaly correlation coefficients (ACC) as follows: CSS = $(\mathrm{ACC}_{\mathrm{hindcast}} - \mathrm{ACC}_{\mathrm{reference}})/(1 - \mathrm{ACC}_{\mathrm{reference}})$ (Murphy, 1988). ACCs are based on observations or observational estimates. Here, we present scores for means of forecast years 2 to 5 of surface air temperature.

A.2.3 Grand Solar Minimum simulations and analysis

Three reference simulations were conducted with fixed solar radiation (based on the CMIP6 piControl solar forcing, as detailed in Matthes et al., 2017), alongside greenhouse gas and ODS concentrations corresponding to the years 1850, 2020, and 2100. In addition, three further simulations were performed, where the atmospheric composition mirrored that of the reference simulations, but a substantial reduction in solar radiation was applied. This solar reduction scenario simulates a dramatic decline in solar energy similar to the Maunder Minimum, based on the scenario described by McCracken and Beer (as outlined in Ergorova et al., 2018). As with the reference simulations, a constant GSM solar forcing was applied. To define this, we calculated the arithmetic mean of the reconstructed Maunder Minimum years (1690–1710) and used the results (for both TSI and SSI) as boundary conditions. All simulations were initialized from a historical simulation at the years 1850, 2020, and 2100. Once the global mean surface temperature reached equilibrium, each model run was extended for an additional 150 years. These years were used to calculate the long-term annual mean of the zonal-mean temperature, 2m temperature, and zonal-mean ocean temperature. GSM-induced anomalies were calculated by subtracting the reference simulation from the GSM integration for the respective period. The p-values were corrected for multiple testing using the Benjamini–Yekutieli procedure (BY-FDR) as implemented in Python's statsmodels.stats.multitest.multipletests. All anomalies were tested for significance using a two-sided Student’s t-test.

Author contributions

TS, WH, JK, TR, FK, SW, MRZ and MS designed and carried out the model experiments. UL has been the main PI of the SOLCHECK project. All authors contributed to the analysis and interpretation of the model data and to the writing of this manuscript.

Competing interests

The authors declare that they have no competing interests.

Acknowledgements

The authors would like to acknowledge NHR-ZIB (Berlin, Germany) and DKRZ (Hamburg, Germany) for generously providing the computational resources for the SOLCHECK project. EMAC model experiments in configuration B were performed on the HoreKa supercomputer, funded by the Ministry of Science, Research and the Arts of Baden-Württemberg and by the German Federal Ministry of Education and Research. We would also like to thank Katja Matthes for serving as lead PI and spokesperson during the first year of the SOLCHECK project.

References

Baumgaertner, A. J. G., Jöckel, P., Riede, H., Stiller, G. P., and Funke, B.: Energetic particle precipitation in ECHAM5/MESSy – Part 2: Solar proton events, Atmos. Chem. Phys., 10, 7285–7302, 2010.

Biastoch, A., Böning, C. W., Getzlaff, J., Molines, J.-M., and Madec, G.: Causes of interannual–decadal variability in the meridional overturning circulation of the mid-latitude North Atlantic Ocean, J. Climate, 21, 6599–6615, https://doi.org/10.1175/2008JCLI2404.1, 2008.

Boer, G. J., Smith, D. M., Cassou, C., Doblas-Reyes, F., Danabasoglu, G., Kirtman, B., Kushnir, Y., Kimoto, M., Meehl, G. A., Msadek, R., Mueller, W. A., Taylor, K. E., Zwiers, F., Rixen, M., Ruprich-Robert, Y., and Eade, R.: The Decadal Climate Prediction Project (DCPP) contribution to CMIP6, Geosci. Model Dev., 9, 3751–3777, https://doi.org/10.5194/gmd-9-3751-2016, 2016.

Camp, C. D. and Tung, K. K.: Surface warming by the solar cycle as revealed by the composite mean difference projection, Geophys. Res. Lett., 34, L14703, https://doi.org/10.1029/2007GL030207, 2007.

Chiodo, G., Oehrlein, J., Polvani, L. M., Fyfe, J. C., and Smith, A. K.: Insignificant influence of the 11-year solar cycle on the North Atlantic Oscillation, Nat. Geosci., 12, 94–99, https://doi.org/10.1038/s41561-018-0293-3, 2019.

Coddington, O., Lean, J., Pilewskie, P., Snow, M., Richard, E., Kopp, G., and Baranyi, T.: Solar irradiance variability: comparisons of models and measurements, Earth Space Sci., 6, 2525–2555, https://doi.org/10.1029/2019EA000693, 2019.

De Jager, C., Akasofu, S.-I., Duhau, S., Livingston, W. C., Nieuwenhuijzen, H., and Potgieter, M. S.: A remarkable recent transition in the solar dynamo, Space Sci. Rev., 201, 109–145, https://doi.org/10.1007/s11214-016-0293-9, 2016.

Dee, D. P., Uppala, S. M., Simmons, A. J., Berrisford, P., Poli, P., Kobayashi, S., Andrae, U., Balmaseda, M. A., Balsamo, G., Bauer, P., Bechtold, P., Beljaars, A. C. M., van de Berg, L., Bidlot, J., Bormann, N., Delsol, C., Dragani, R., Fuentes, M., Geer, A. J., Haimberger, L., Healy, S. B., Hersbach, H., Hólm, E. V., Isaksen, L., Kållberg, P., Köhler, M., Matricardi, M., McNally, A. P., Monge-Sanz, B. M., Morcrette, J.-J., Park, B.-K., Peubey, C., de Rosnay, P., Tavolato, C., Thépaut, J.-N., and Vitart, F.: The ERA-Interim reanalysis: configuration and performance of the data assimilation system, Q. J. Roy. Meteor. Soc., 137, 553–597, https://doi.org/10.1002/qj.828, 2011.

Drews, A., Huo, W., Matthes, K., Kodera, K., and Kruschke, T.: The Sun's role in decadal climate predictability in the North Atlantic, Atmos. Chem. Phys., 22, 7893–7904, https://doi.org/10.5194/acp-22-7893-2022, 2022.

Eddy, J. A.: The Maunder Minimum: The reign of Louis XIV appears to have been a time of real anomaly in the behavior of the Sun, Science, 192, 1189–1202, https://doi.org/10.1126/science.192.4245.1189, 1976.

Egorova, T., Schmutz, W., Rozanov, E., Shapiro, A. I., Usoskin, I., Beer, J., Tagirov, R., and Peter, T.: Revised historical solar irradiance forcing, Astron. Astrophys., 615, A85, https://doi.org/10.1051/0004-6361/201731199, 2018.

Eyring, V., Bony, S., Meehl, G. A., Senior, C. A., Stevens, B., Stouffer, R. J., and Taylor, K. E.: Overview of the Coupled Model Intercomparison Project Phase 6 (CMIP6) experimental design and organization, Geosci. Model Dev., 9, 1937–1958, https://doi.org/10.5194/gmd-9-1937-2016, 2016.

Fichefet, T., and Maqueda, M. A. M.: Sensitivity of a global sea ice model to the treatment of ice thermodynamics and dynamics, J. Geophys. Res.-Oceans, 102, 12609–12646, https://doi.org/10.1029/97JC00480, 1997.

Fiedler, S., Stevens, B., and Mauritsen, T.: On the sensitivity of anthropogenic aerosol forcing to model-internal variability and parameterizing a Twomey effect, J. Adv. Model. Earth Syst., 9, 1325–1341, https://doi.org/10.1002/2017MS000932, 2017.

Funke, B., López-Puertas, M., Stiller, G. P., and von Clarmann, T.: Mesospheric and stratospheric NOy produced by energetic particle precipitation during 2002–2012, J. Geophys. Res. Atmos., 119, 4429–4446, https://doi.org/10.1002/2013JD021404, 2014.

Funke, B., Baumgaertner, A., Calisto, M., Egorova, T., Jackman, C. H., Kieser, J., Krivolutsky, A., López-Puertas, M., Marsh, D. R., Reddmann, T., Rozanov, E., Salmi, S.-M., Sinnhuber, M., Stiller, G. P., Verronen, P. T., Versick, S., von Clarmann, T., Vyushkova, T. Y., Wieters, N., and Wissing, J. M.: Composition changes after the "Halloween" solar proton event: the High Energy Particle Precipitation in the Atmosphere

(HEPPA) model versus MIPAS data intercomparison study, Atmos. Chem. Phys., 11, 9089–9139, https://doi.org/10.5194/acp-11-9089-2011, 2011.

Funke, B., López-Puertas, M., Stiller, G. P., Versick, S., and von Clarmann, T.: A semi-empirical model for mesospheric and stratospheric NOy produced by energetic particle precipitation, Atmos. Chem. Phys., 16, 8667–8693, https://doi.org/10.5194/acp-16-8667-2016, 2016.

Funke, B., Ball, W., Bender, S., Gardini, A., Harvey, V. L., Lambert, A., López-Puertas, M., Marsh, D. R., Meraner, K., Nieder, H., Päivärinta, S.-M., Pérot, K., Randall, C. E., Reddmann, T., Rozanov, E., Schmidt, H., Seppälä, A., Sinnhuber, M., Sukhodolov, T., Stiller, G. P., Tsvetkova, N. D., Verronen, P. T., Versick, S., von Clarmann, T., Walker, K. A., and Yushkov, V.: HEPPA-II model–measurement intercomparison project: EPP indirect effects during the dynamically perturbed NH winter 2008–2009, Atmos. Chem. Phys., 17, 3573–3604, https://doi.org/10.5194/acp-17-3573-2017, 2017.

Giorgetta, M. A., and Bengtsson, L.: Potential role of the quasi-biennial oscillation in the stratosphere–troposphere exchange as found in water vapour in general circulation model experiments, J. Geophys. Res. Atmos., 104, 6003–6019, https://doi.org/10.1029/1998JD200120, 1999.

Giorgetta, M. A., Manzini, E., Roeckner, E., Esch, M., and Bengtsson, L.: Climatology and forcing of the quasi-biennial oscillation in the MAECHAM5 model, J. Climate, 19, 3882–3901, https://doi.org/10.1175/JCLI3830.1, 2006.

Hegglin, M., Kinnison, D., Lamarque, J.-F., and Plummer, D.: CCMI ozone in support of CMIP6 – version 1.0, Earth Syst. Grid Fed., https://doi.org/10.22033/ESGF/input4MIPs.1115, 2016.

Iacono, M. J., Delamere, J. S., Mlawer, E. J., Shephard, M. W., Clough, S. A., and Collins, W. D.: Radiative forcing by long-lived greenhouse gases: Calculations with the AER radiative transfer models, J. Geophys. Res. Atmos., 113, D13103, https://doi.org/10.1029/2008JD009944, 2008.

Ilyina, T., Six, K. D., Segschneider, J., Maier-Reimer, E., Li, H., and Núñez-Riboni, I.: Global ocean biogeochemistry model HAMOCC: Model architecture and performance as component of the MPI Earth System Model in different CMIP5 experimental realizations, J. Adv. Model. Earth Syst., 5, 287–315, https://doi.org/10.1029/2012MS000178, 2013.

Jöckel, P., Kerkweg, A., Pozzer, A., Sander, R., Tost, H., Riede, H., Baumgaertner, A., Gromov, S., and Kern, B.: Development cycle 2 of the Modular Earth Submodel System (MESSy2), Geosci. Model Dev., 3, 717–752, https://doi.org/10.5194/gmd-3-717-2010, 2010.

Jöckel, P., Tost, H., Pozzer, A., Kunze, M., Kirner, O., Brenninkmeijer, C. A. M., Brinkop, S., Cai, D. S., Dyroff, C., Eckstein, J., Frank, F., Garny, H., Gottschaldt, K.-D., Graf, P., Grewe, V., Kerkweg, A., Kern, B., Matthes, S., Mertens, M., Meul, S., Neumaier, M., Nützel, M., Oberländer-Hayn, S., Ruhnke, R., Runde, T., Sander, R., Scharffe, D., Zahn, A., and Ziereis, H.: Earth system chemistry integrated modelling (ESCiMo) with the Modular Earth Submodel System (MESSy) version 2.51, Geosci. Model Dev., 9, 1153–1200, https://doi.org/10.5194/gmd-9-1153-2016, 2016.

Jungclaus, J. H., Keenlyside, N., Botzet, M., Haak, H., Luo, J.-J., Latif, M., Marotzke, J., Mikolajewicz, U., Notz, D., and Roeckner, E.: Ocean circulation and tropical variability in the coupled model ECHAM5/MPI-OM, J. Climate, 19, 3952–3972, https://doi.org/10.1175/JCLI3815.1, 2006.

Jungclaus, J. H., Fischer, N., Haak, H., Lohmann, K., Marotzke, J., Matei, D., Mikolajewicz, U., Notz, D., and von Storch, J.-S.: Characteristics of the ocean simulations in MPIOM, the ocean component of the MPI Earth System Model, J. Adv. Model. Earth Syst., 5, 422–446, https://doi.org/10.1002/jame.20023, 2013.

Kinnison, D. E., Brasseur, G. P., Walters, S., Garcia, R. R., Marsh, D. R., Sassi, F., Harvey, V. L., Randall, C. E., Emmons, L., Lamarque, J.-F., Hess, P., Orlando, J. J., Tie, X. X., Randel, W., Pan, L. L., Gettelman, A., Granier, C., Diehl, T., Niemeier, U., and Simmons, A. J.: Sensitivity of chemical tracers to meteorological parameters in the MOZART-3 chemical transport model, J. Geophys. Res. Atmos., 112, D20302, https://doi.org/10.1029/2006JD007879, 2007.

Kodera, K.: Solar cycle modulation of the North Atlantic Oscillation: implication in the spatial structure of the NAO, Geophys. Res. Lett., 29, 1218, https://doi.org/10.1029/2001GL014557, 2002.

Kodera, K., and Kuroda, Y.: Dynamical response to the solar cycle, J. Geophys. Res. Atmos., 107, ACL 5-1–ACL 5-12, https://doi.org/10.1029/2002JD002224, 2002.

Kouker, W., Langbein, I., Reddmann, T., and Ruhnke, R.: The Karlsruhe Simulation Model of the Middle Atmosphere Version 2, Wiss. Ber. FZKA 6278, Forschungszentrum Karlsruhe, Karlsruhe, Germany, 1999.

Kunze, M., Godolt, M., Langematz, U., Grenfell, J. L., Hamann-Reinus, A., and Rauer, H.: Investigating the early Earth faint young Sun problem with a general circulation model, Planet. Space Sci., 98, 77–92, https://doi.org/10.1016/j.pss.2014.01.008, 2014.

Langematz, U., Claussnitzer, A., Matthes, K., and Kunze, M.: The climate during the Maunder Minimum: a simulation with the Freie Universität Berlin Climate Middle Atmosphere Model (FUB-CMAM), J. Atmos. Sol. Terr. Phys., 67, 55–69, https://doi.org/10.1016/j.jastp.2004.07.017, 2005.

Lenssen, N. J. L., Schmidt, G. A., Hansen, J. E., Menne, M. J., Persin, A., Ruedy, R., and Zyss, D.: Improvements in the GISTEMP uncertainty model, J. Geophys. Res. Atmos., 124, 6307–6326, https://doi.org/10.1029/2018JD029522, 2019.

Luterbacher, J., Rickli, R., Xoplaki, E., Tinguely, C., Beck, C., Pfister, C., and Wanner, H.: The late Maunder Minimum (1675–1715) – a key period for studying decadal scale climatic change in Europe, Clim. Change, 49, 441–462, https://doi.org/10.1023/A:1010667524422, 2001.

Madec, G.: NEMO ocean engine, Note du Pôle Modélisation, Inst. Pierre-Simon Laplace, 406 pp., ISSN 1288-1619, 2016.

Maliniemi, V., Asikainen, T., and Mursula, K.: Spatial distribution of Northern Hemisphere winter temperatures during different phases of the solar cycle, J. Geophys. Res. Atmos., 119, 9752–9764, https://doi.org/10.1002/2013JD021343, 2014.

Maliniemi, V., Asikainen, T., Salminen, A., and Mursula, K.: Assessing North Atlantic winter climate response to geomagnetic activity and solar irradiance variability, Q. J. Roy. Meteorol. Soc., 145, 3780–3789, https://doi.org/10.1002/qj.3657, 2019.

Marotzke, J., Müller, W. A., Vamborg, F. S. E., Becker, P., Cubasch, U., Feldmann, H., Kaspar, F., Kottmeier, C., Marini, C., Polkova, I., Prömmel, K., Rust, H. W., Stammer, D., Ulbrich, U., Kadow, C., Köhl, A., Kröger, J., Kruschke, T., Pinto, J. G., Pohlmann, H., Reyers, M., Schröder, M., Sienz, F., Timmreck, C., and Ziese, M.: MiKlip – a national research project on decadal climate prediction, Bull. Am. Meteorol. Soc., 97, 2379–2394, https://doi.org/10.1175/BAMS-D-15-00184.1, 2016.

Matthes, K., Funke, B., Andersson, M. E., Barnard, L., Beer, J., Charbonneau, P., Clilverd, M. A., Dudok de Wit, T., Haberreiter, M., Hendry, A., Jackman, C. H., Kretzschmar, M., Kruschke, T., Kunze, M., Langematz, U., Marsh, D. R., Maycock, A. C., Misios, S., Rodger, C. J., Scaife, A. A., Seppälä, A., Shangguan, M., Sinnhuber, M., Tourpali, K., Usoskin, I., Van de Kamp, M., Verronen, P. T., and Versick, S.: Solar forcing for CMIP6 (v3.2), Geosci. Model Dev., 10, 2247–2302, https://doi.org/10.5194/gmd-10-2247-2017, 2017.

Matthes, K., Biastoch, A., Wahl, S., Harlaß, J., Martin, T., Brücher, T., Drews, A., Ehlert, D., Getzlaff, K., Krüger, F., Rath, W., Scheinert, M., Schwarzkopf, F. U., Bayr, T., Schmidt, H., and Park, W.: The Flexible Ocean and Climate Infrastructure version 1 (FOCI1): mean state and variability, Geosci. Model Dev., 13, 2533–2568, https://doi.org/10.5194/gmd-13-2533-2020, 2020.

Meinshausen, M., Vogel, E., Nauels, A., Lorbacher, K., Meinshausen, N., Etheridge, D. M., et al.: Historical greenhouse gas concentrations for climate modelling (CMIP6), Geosci. Model Dev., 10, 2057–2116, https://doi.org/10.5194/gmd-10-2057-2017, 2017.

Mekhaldi, F., Muscheler, R., Adolphi, F., Aldahan, A., Beer, J., McConnell, J. R., Possnert, G., Sigl, M., Svensson, A., Synal, H.-A., Welten, K. C., and Woodruff, T. E.: Multiradionuclide evidence for the solar origin of the cosmic-ray events of AD 774/5 and 993/4, Nat. Commun., 6, 8611, https://doi.org/10.1038/ncomms9611, 2015.

Miyake, F., Nagaya, K., Masuda, K., and Nakamura, T.: A signature of cosmic-ray increase in AD 774–775 from tree rings in Japan, Nature, 486, 240–242, https://doi.org/10.1038/nature11123, 2012.

Müller, W. A., Jungclaus, J. H., Mauritsen, T., Baehr, J., Bittner, M., Budich, R., Bunzel, F., Esch, M., Ghosh, R., Haak, H., Ilyina, T., Kleine, T., Kornblueh, L., Li, H., Modali, K., Notz, D., Pohlmann, H., Roeckner, E., Stemmler, I., and Marotzke, J.: A higher-resolution version of the Max Planck Institute Earth System Model (MPI-ESM1.2-HR), J. Adv. Model. Earth Syst., 10, 1383–1413, https://doi.org/10.1029/2017MS001217, 2018.

Murphy, A. H.: Skill scores based on the mean square error and their relationships to the correlation coefficient, Mon. Weather Rev., 116, 2417–2424, 1988.

Pincus, R., and Stevens, B.: Paths to accuracy for radiation parameterizations in atmospheric models, J. Adv. Model. Earth Syst., 5, 225–233, https://doi.org/10.1002/jame.20027, 2013.

Pohlmann, H., Müller, W. A., Bittner, M., Hettrich, S., Modali, K., Pankatz, K., and Marotzke, J.: Realistic quasi-biennial oscillation variability in the historical and hindcast simulations using CMIP6 forcing, Geophys. Res. Lett., 46, 14118–14125, https://doi.org/10.1029/2019GL084878, 2019.

Rahmanifard, F., Jordan, A. P., De Wet, W. C., Schwadron, N. A., Wilson, J. K., Owens, M. J., Joyce, C. J., and Riley, P.: Evidence from galactic cosmic rays that the Sun has likely entered a secular minimum in solar activity, Space Weather, 20, e2021SW002796, https://doi.org/10.1029/2021SW002796, 2022.

Randall, C. E., Harvey, V. L., Singleton, C. S., Bailey, S. M., Bernath, P. F., Codrescu, M., Nakajima, H., and Russell, J. M. III: Energetic particle precipitation effects on the Southern Hemisphere stratosphere in 1992–2005, J. Geophys. Res. Atmos., 112, D08308, https://doi.org/10.1029/2006JD007696, 2007.

Reddmann, T., Sinnhuber, M., Wissing, J. M., Yakovchuk, O., and Usoskin, I.: The impact of an extreme solar event on the middle atmosphere: a case study, Atmos. Chem. Phys., 23, 6989–7000, https://doi.org/10.5194/acp-23-6989-2023, 2023.

Reick, C. H., Raddatz, T., Brovkin, V., and Gayler, V.: The representation of natural and anthropogenic land cover change in MPI-ESM, J. Adv. Model. Earth Syst., 5, 459–482, https://doi.org/10.1002/jame.20022, 2013.

Rimbu, N., Spiegl, T. C., Ionita, M., Doshi, S., and Lohmann, G.: A synoptic scale perspective of solar forcing on extreme precipitation and floods over Europe during summer, J. Geophys. Res. Atmos., 129, e2024JD041952, https://doi.org/10.1029/2024JD041952, 2024.

Rind, D., Lean, J., and Healy, R.: Simulated time-dependent climate response to solar radiative forcing since 1600, J. Geophys. Res., 104, 1973–1990, https://doi.org/10.1029/1998JD200020, 1999.

Roeckner, E., Brokopf, R., Esch, M., Giorgetta, M. A., Hagemann, S., Kornblueh, L., Manzini, E., Schlese, U., and Schulzweida, U.: Sensitivity of simulated climate to horizontal and vertical resolution in the ECHAM5 atmosphere model, J. Climate, 19, 3771–3791, https://doi.org/10.1175/JCLI3824.1, 2006.

Sander, R., Baumgaertner, A., Gromov, S., Harder, H., Jöckel, P., Kerkweg, A., Kubistin, D., Regelin, E., Riede, H., Sandu, A., Taraborrelli, D., Tost, H., and Xie, Z.-Q.: The atmospheric chemistry box model CAABA/MECCA-3.0, Geosci. Model Dev., 4, 373–380, https://doi.org/10.5194/gmd-4-373-2011, 2011.

Sander, R., Jöckel, P., Kirner, O., Kunert, A. T., Landgraf, J., and Pozzer, A.: The photolysis module JVAL-14, compatible with the MESSy standard, and the JVal PreProcessor (JVPP), Geosci. Model Dev., 7, 2653–2662, https://doi.org/10.5194/gmd-7-2653-2014, 2014.

Schmidt, H., Brasseur, G. P., Charron, M., Manzini, E., Giorgetta, M. A., Diehl, T., Fomichev, V. I., Kinnison, D., Marsh, D., and Walters, S.: The HAMMONIA Chemistry Climate Model: Sensitivity of the mesopause region to the 11-year solar cycle and CO2 doubling, J. Climate, 19, 3903–3931, https://doi.org/10.1175/JCLI3829.1, 2006.

Schultz, M. G., Stadtler, S., Schröder, S., Taraborrelli, D., Franco, B., Krefting, J., Henrot, A., Ferrachat, S., Lohmann, U., Neubauer, D., Siegenthaler-Le Drian, C., Wahl, S., Kokkola, H., Kühn, T., Rast, S., Schmidt, H., Stier, P., Kinnison, D., Tyndall, G. S., Orlando, J. J., and Wespes, C.: The chemistry–climate model ECHAM6.3-HAM2.3-MOZ1.0, Geosci. Model Dev., 11, 1695–1723, https://doi.org/10.5194/gmd-11-1695-2018, 2018.

Sedlacek, J., Sukhodolov, T., Egorova, T., Karagodin-Doyennel, A., and Rozanov, E.: Future climate under CMIP6 solar activity scenarios, Earth Space Sci., 10, e2022EA002783, https://doi.org/10.1029/2022EA002783, 2023.

Seppälä, A., Randall, C. E., Clilverd, M. A., Rozanov, E., and Rodger, C. J.: Geomagnetic activity and polar surface air temperature variability, J. Geophys. Res. Space Phys., 114, A10312, https://doi.org/10.1029/2008JA014029, 2009.

Sinnhuber, M., Nieder, H., and Wieters, N.: Energetic particle precipitation and the chemistry of the mesosphere/lower thermosphere, Surv. Geophys., 33, 1281–1334, https://doi.org/10.1007/s10712-012-9201-3, 2012.

Sinnhuber, M., Berger, U., Funke, B., Nieder, H., Reddmann, T., Stiller, G., Versick, S., von Clarmann, T., and Wissing, J. M.: NOy production, ozone loss and changes in net radiative heating due to energetic particle precipitation in 2002–2010, Atmos. Chem. Phys., 18, 1115–1147, https://doi.org/10.5194/acp-18-1115-2018, 2018.

Sinnhuber, M., and Funke, B.: Energetic electron precipitation into the atmosphere, in: The Dynamic Loss of Earth's Radiation Belts, edited by: Allison, H. J., Elsevier, Amsterdam, 279–321, https://doi.org/10.1016/B978-9-12-813371-2.00009-3, 2019.

Sinnhuber, M., Nesse Tyssøy, H., Asikainen, T., Bender, S., Funke, B., Hendrickx, K., Pettit, J. M., Reddmann, T., Rozanov, E., Schmidt, H., Smith-Johnsen, C., Sukhodolov, T., Szeląg, M. E., van de Kamp, M., Verronen, P. T., Wissing, J. M., and Yakovchuk, O. S.: Heppa III Intercomparison Experiment on Electron Precipitation Impacts: 2. Model–measurement intercomparison of nitric oxide (NO) during a geomagnetic storm in April 2010, J. Geophys. Res. Space Phys., 127, e2021JA029466, https://doi.org/10.1029/2021JA029466, 2021.

Sinnhuber, M., Arras, C., Bender, S., Funke, B., Liu, H., Marsh, D. R., and Wissing, J. M.: Thermospheric nitric oxide is modulated by the ratio of atomic to molecular oxygen and thermospheric dynamics during solar minimum, Atmos. Chem. Phys., 25, 14719–14734, 2025.

Siskind, D. E., Jones Jr., M., and Reep, J. W.: Effects of supernova-induced soft X-rays on middle- and upper-atmospheric nitric oxide and stratospheric ozone, Ann. Geophys., 43, 201–216, https://doi.org/10.5194/angeo-43-201-2025, 2025.

Spiegl, T. C., Langematz, U., Pohlmann, H., and Kröger, J.: A critical evaluation of decadal solar cycle imprints in the MiKlip historical ensemble simulations, Weather Clim. Dynam., 4, 789–807, https://doi.org/10.5194/wcd-4-789-2023, 2023.

Spiegl, T., and Langematz, U.: Twenty-first-century climate change hot spots in the light of a weakening Sun, J. Climate, 33, 3431–3447, https://doi.org/10.1175/JCLI-D-19-0059.1, 2020.

Stevens, B., Fiedler, S., Kinne, S., Peters, K., Rast, S., Müsse, J., and Mauritsen, T.: MACv2-SP: A parameterization of anthropogenic aerosol optical properties and an associated Twomey effect for use in CMIP6, Geosci. Model Dev., 10, 433–452, https://doi.org/10.5194/gmd-10-433-2017, 2017.

Stevens, B., Giorgetta, M., Esch, M., Mauritsen, T., Crueger, T., Rast, S., Salzmann, M., Schmidt, H., Bader, J., Block, K., Brokopf, R., Fast, I., Kinne, S., Kornblueh, L., Lohmann, U., Pincus, R., Reichler, T., and Roeckner, E.: Atmospheric component of the MPI-M Earth System Model: ECHAM6, J. Adv. Model. Earth Syst., 5, 146–172, https://doi.org/10.1002/jame.20015, 2013.

Thiéblemont, R., Matthes, K., Omrani, N.-E., Kodera, K., and Hansen, F.: Solar forcing synchronizes decadal North Atlantic climate variability, Nat. Commun., 6, 8268, https://doi.org/10.1038/ncomms9268, 2015.

Thomason, L. W., Ernest, N., Millán, L., Rieger, L., Bourassa, A., Vernier, J.-P., Manney, G., Luo, B., Arfeuille, F., and Peter, T.: A global space-based stratospheric aerosol climatology: 1979–2016, Earth Syst. Sci. Data, 10, 469–492, https://doi.org/10.5194/essd-10-469-2018, 2018.

Usoskin, I. G., Sokoloff, D., and Moss, D.: Grand minima of solar activity and the mean field dynamo, Sol. Phys., 254, 345–355, https://doi.org/10.1007/s11207-008-9293-6, 2009.

Usoskin, I. G.: A history of solar activity over millennia, Living Rev. Sol. Phys., 20, 2, https://doi.org/10.1007/s41116-023-00036-z, 2023a.

Usoskin, I., Miyake, F., Baroni, M., Brehm, N., Dalla, S., Hayakawa, H., Hudson, H., Jull, A. J. T., Knipp, D., Koldobskiy, S., Maehara, H., Mekhaldi, F., Notsu, Y., Poluianov, S., Rozanov, E., Shapiro, A., Spiegl, T., Sukhodolov, T., Uusitalo, J., and Wacker, L.: Extreme solar events: setting up a paradigm, Space Sci. Rev., 219, 73, https://doi.org/10.1007/s11214-023-01018-1, 2023b.

Wissing, J. M., and Kallenrode, M.-B.: Atmospheric Ionization Module Osnabrück (AIMOS): a 3-D model to determine atmospheric ionization by energetic charged particles from different populations, J. Geophys. Res. Space Phys., 114, A06104, https://doi.org/10.1029/2008JA013884, 2009.

Zorita, E., von Storch, H., Gonzalez-Rouco, F. J., Cubasch, U., Luterbacher, J., Legutke, S., Fischer-Bruns, I., and Schlese, U.: Climate evolution in the last five centuries simulated by an atmosphere-ocean model: global temperatures, the North Atlantic Oscillation and the Late Maunder Minimum, Meteorol. Z., 13, 271–289, https://doi.org/10.1127/0941-2948/2004/0013-0271, 2004.